Principal Modes of Rainfall–SST Variability of the Asian Summer Monsoon: A Reassessment of the Monsoon–ENSO Relationship

K.-M. LAU AND H. T. WU

Climate and Radiation Branch, NASA Goddard Space Flight Center, Greenbelt, Maryland

(Manuscript received 7 March 2000, in final form 26 September 2000)

ABSTRACT

Using global rainfall and sea surface temperature (SST) data for the past two decades (1979–98), the covariability of the Asian summer monsoon (ASM) and El Niño–Southern Oscillation (ENSO) was investigated. The findings suggest three recurring rainfall–SST coupled modes. Characterized by a pronounced biennial variability, the first mode is associated with generally depressed rainfall over the western Pacific and the ''Maritime Continent,'' stemming from the eastward shift of the Walker circulation during the growth phase of El Niño. The associated SST pattern consists of an east–west SST seesaw across the Pacific and another seesaw with opposite polarity over the Indian Ocean. The second mode is associated with a growing La Niña, comprising mixed, regional, and basin-scale rainfall and SST variability with abnormally warm water in the vicinity of the Maritime Continent and western Pacific. It possesses a pronounced low-level west Pacific anticyclone (WPA) near the Philippines and exhibits large subseasonal-scale variability. The third mode is associated with regional coupled ocean–atmosphere processes in the ASM region, having spatial and temporal variabilities that suggest extratropical linkages and interhemispheric interactions occurring on decadal timescales.

Results indicate the importance of regional processes in affecting ASM rainfall variability. On the average, and over the ASM region as a whole, ENSO-related basin-scale SSTs can account for about 30% of the variability, and regional processes can account for an additional 20%. In individual years and over subregions, the percentages can be much higher or lower. In addition to the shift in the Walker circulation, it is found that the regional excitation of the WPA is important in determining the rainfall variability over south Asia and east Asia. Based on the results, a hypothesis is proposed that anomalous wind forcings derived from the WPA may be instrumental in inducing a biennial modulation to natural ENSO cycles. The causes of the 1997 and 1998 rainfall anomalies over the ASM subregions are discussed in the context of these results and in light of recent observations of long-term changes in the monsoon–ENSO relationship.

1. Introduction

The Asian summer monsoon (ASM) is subject to large interannual fluctuations causing floods and droughts of varying degrees of severity in different ASM subregions. During the summer of 1998, the great flood of the Yangtze River was one of the worst natural disasters on record (3700 deaths, 223 million people displaced, and property damages up to $30 billion). In the same year, excessive monsoon rainfall also caused severe flooding over Bangladesh (30 million people displaced and property damages up to $3.4 billion). Yet, one year before, in the summer of 1997, the above regions had nearly normal summer rainfall, but northern China experienced record drought conditions. Southern China was gripped by widespread flooding, while the average rainfall over the entire Indian subcontinent was nearly normal.

Corresponding author address: Dr. William K.-M. Lau, Climate and Radiation Branch, NASA Goddard Space Flight Center, Greenbelt, MD 20771.
E-mail: lau@climate.gsfc.nasa.gov

The extreme climate shifts do not seem to be consistent with expectations based on many previous studies that indicate a weak (strong) ASM is associated with the warm (cold) phase of the El Niño–Southern Oscillation (ENSO; Rasmusson and Carpenter 1983; Shukla and Paolino 1983; Webster and Yang 1992; Lau and Yang 1996; Ju and Slingo 1995; and many others). Various factors have been suggested to ''explain'' the discrepancies between the observed and the expected. These factors range from the possible impacts on monsoon rainfall anomalies by intraseasonal oscillations, the tropospheric biennial oscillation, Indian Ocean sea surface temperature (SST) anomalies, Eurasian snow cover, to decadal changes in ENSO monsoon coupling and global warming. These factors have been the subject of a large number of recent investigations (Lau and Weng 2001; Wang et al. 2000; Webster et al. 1999; Chandrasekar and Kitoh 1998; Shen and Kimoto 1999; Goswami et al. 1998; Li and Yanai 1996; Meehl and Arblaster 1998; Meehl 1997; Shen and Lau 1995; and many others). As yet, there are no conclusive results regarding the relative importance of each of the factors in con-

tributing to the ASM anomalies and how they may have impacted the monsoon–ENSO relationship.

One of the reasons for the aforementioned conundrum is that both monsoon and ENSO are inherently complex phenomena, governed by the interplay of a large number of physical processes with different spatial and temporal scales. Because of the nonlinear nature of the complex interactions, the monsoon–ENSO relationship is most likely to be nonstationary, being strongly modulated by decadal or longer timescale variability (Torrence and Webster 1999; Kumar et al. 1999; Krishnamurthy and Goswami 2000). Another reason may have to do with the difficulty in defining monsoon variability. Most previous monsoon–ENSO studies were based on ad hoc indices, usually derived from rainfall variability for a monsoon subregion (e.g., the all-India monsoon rainfall index) or from the large-scale wind field to describe the broad-scale monsoon variability (e.g., Webster and Yang 1992). Results based on these indices may have oversimplified the problem. Recently, a number of investigators have pointed out the need to better define the regionality of the monsoon from dynamics-based indices (Goswami et al. 1999; Wang and Fan 1999; and Wang et al. 2000). Lau et al. (2000) demonstrated that, based on the regional characteristics of atmospheric dynamics and lower boundary forcings, at least two major subcomponents of the ASM—the south Asian monsoon (SAM) and the east Asian monsoon (EAM)—need to be distinguished in monsoon–ENSO studies. In a pilot study to assess the regional impacts of the 1997/98 El Niño on the Asian–Australia monsoon, Lau and Wu (1999) found that both regional and basin-scale processes contributed significantly to the observed all-ASM rainfall anomalies in 1997. Miyakoda et al. (1999) found that the monsoon–ENSO relationship may depend on the ambient state of the Walker circulation.

In this paper, we focus on the identification and physical interpretation of intrinsic monsoon–SST modes and the quantitative evaluation of factors contributing to ASM rainfall anomalies in individual years. Unlike previous monsoon–ENSO studies, which mostly viewed the monsoon from the vantage point of El Niño, here we reexamine the monsoon–ENSO relationship based on a ''monsoon-centric'' viewpoint. We will not use specific monsoon indices; rather, we describe monsoon variability over the ASM region as a whole to identify physically meaningful and robust intrinsic modes, and then consider the subregional variability based on these modes. In section 2, we provide a brief description of the data used. We cite examples of spatial and temporal variability of the observed rainfall and SST in the ASM region to help us to pose relevant scientific questions in section 3. We then identify and provide physical interpretations to various recurring monsoon rainfall–SST modes using Singular Value Decomposition (SVD) analysis in section 4. In section 5, we use the identified modes to estimate potential predictability, and to determine relative roles of various physical processes in contributing to the year-by-year observed rainfall anomalies. In section 6, we propose a hypothesis on the possible impact of ASM on the evolution of ENSO cycles. The conclusions and further discussion of these results in light of other related work are presented in section 7.

2. Data and analysis procedure

The present analysis is based on historical rainfall, SST, and reanalysis of wind data. For rainfall, we use the Climate Prediction Center (CPC) Merged Analysis Precipitation (CMAP) satellite–gauge monthly product with $2.5° \times 2.5°$ resolution for the period 1979–98 (Xie and Arkin 1997). For SST, we use the optimally gridded $2° \times 2°$ product of Reynolds and Smith (1994) for the same period. SVD is used to identify coupled modes of rainfall and SST globally (40°S–40°N), over the ASM domain (20°S–40°N, 30°–150°E), and for different combinations of rainfall and SST domains to ensure the robustness of the modes. Although we focus on June–July–August (JJA) for the main discussions, we use the 5-month period from May through September (MJJAS) in the statistical analysis to include the extended boreal summer season and to increase sampling. We use the National Centers for Environmental Prediction–National Center for Atmospheric Research wind reanalysis (Kalnay et al. 1996) to aid in the physical interpretation of the coupled modes identified by the SVD analysis. To ensure that our results are not affected by one major episode, we have carried out identical SVD analysis for both the 20-yr period and for the 19-yr period (excluding 1998). Since the two analyses yield almost identical qualitative results, only results for the full period are shown in the main text. Examples of results for the 19-yr data are presented in the appendix.

3. ASM rainfall and SST anomalies

In this section, we use ASM rainfall and SST observations to highlight a number of key scientific questions germane to the present analysis. As an example, Figs. 1a and 1b show the complex and highly localized structure of the rainfall anomalies during July 1997 and 1998. These rainfall anomalies tend to be anchored to local topography of the Bay of Bengal, the South China Sea, the Arabian Sea, and the ''Maritime Continent.'' In comparison with those of 1997, the 1998 anomalies seem to show more large-scale organization. Notice that the record floods in Bangladesh and in the Yantze River Valley in 1998 appear only as two of the many small-scale features in the rainfall anomaly field. In July 1997, the SST adjacent to the Maritime Continent is below normal, while the Indian Ocean is slightly above normal, except near the western Indian Ocean between 10° and 20°S (Fig. 1c). In July 1998, the SST anomaly in the vicinity of the Maritime Continent and the eastern Indian Ocean reversed its sign to become strongly above normal, while the Indian Ocean SST as a

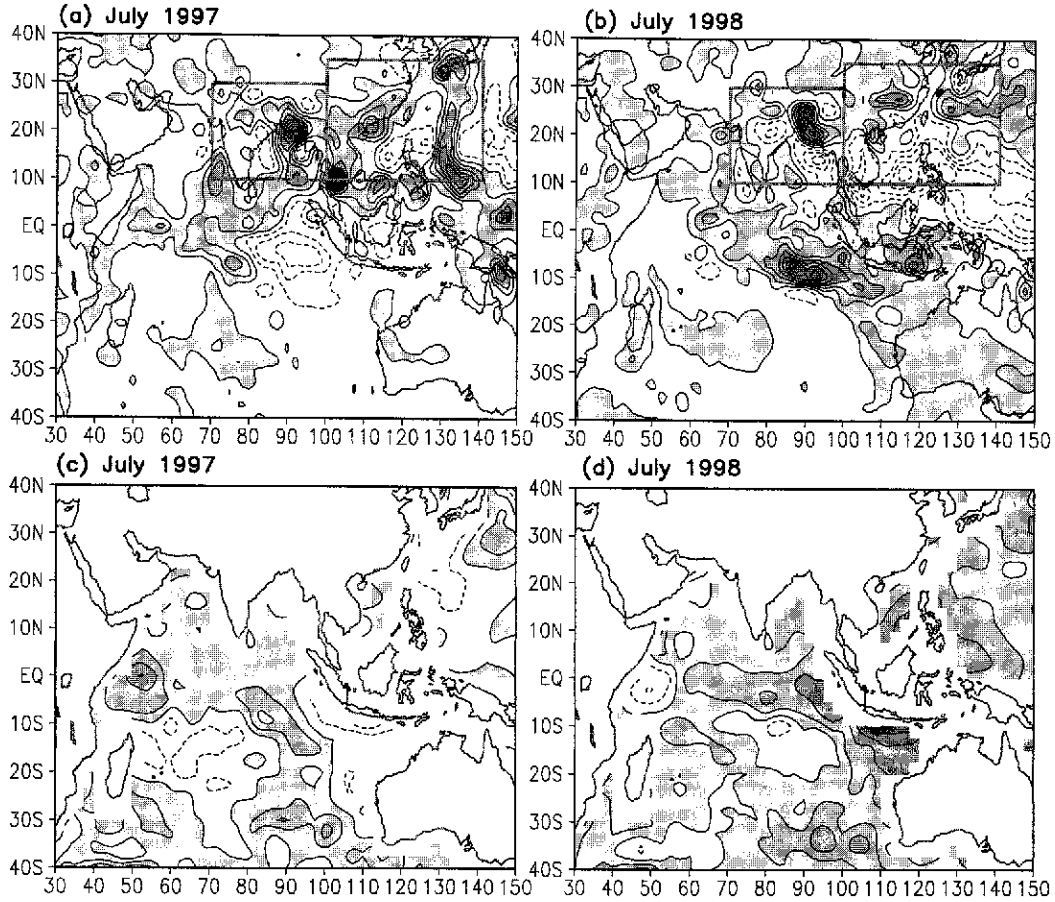

FIG. 1. Observed (a)(b) rainfall and (c)(d) SST anomalies during Jul 1997 and 1998. Contour interval for rainfall is 2 mm day^{-1} and for SST is 0.5°C. Regions with positive values are shaded. The range for rainfall anomalies is -6 to 16 mm day^{-1} and for SST is $-1°$ to 2°C.

whole remained generally above normal (Fig. 1d). The month-to-month variability of the ASM rainfall and SST anomalies were also very large (not shown).

Figures 2a and 2b show the time–longitude sections along the equator of monthly rainfall and SST anomalies from January 1979 through December 1998. The most prominent feature is the eastward extension of the rainfall anomalies from the central Pacific to the coast of South America concomitant with the development of warm water over the equatorial eastern Pacific during the El Niño of 1982/83, 1986/87, 1991/92, and 1997/98. As a result, an east–west dipole rainfall anomaly develops between the central-eastern Pacific and the Maritime Continent (Fig. 2a). This rainfall pattern is associated with the well-known eastward shift of the Walker circulation, associated with an El Niño. Strong intraseasonal oscillations in rainfall (Fig. 2a), and, to a much lesser extent in SST (Fig. 2b), are found in the ASM sector. These intraseasonal oscillations appear as somewhat discontinuous, eastward-propagating signals originating from the far western Indian Ocean and terminating near the date line, except during an El Niño, when they reach the far eastern Pacific.

Notice that a well-defined La Niña developed in the latter part of 1988 and 1998, in the form of a sharp biennial reversal in the SST anomalies in the eastern Pacific, following the 1986/87 and the 1997/98 El Niño. However, following the 1982/83 El Niño, a weaker cold phase lingered on for more than two years. Likewise, after the 1991/92 El Niño, a weak and protracted cold phase, interspersed with two weak warm events (in 1993 and 1995), developed. Also note the extraordinary warmth (>1°C SST anomaly) of the Indian Ocean and the establishment of a strong east–west dipole in rainfall and SST between the eastern and western Indian Ocean during the latter part of 1997 and early part of 1998. Yu and Rienecker (1999) and Webster et al. (1999) noted these features in their recent reports.

The diverse spatial and temporal scales in the ASM rainfall and SST anomalies raise the following questions: How much of the observed anomalies in individual events, for example, 1997/98, are the results of direct impacts from El Niño and La Niña? How much arise from regional coupled processes? To what extent are these anomalies predictable? Additional questions are, What causes the sharp biennial reversal in SST in con-

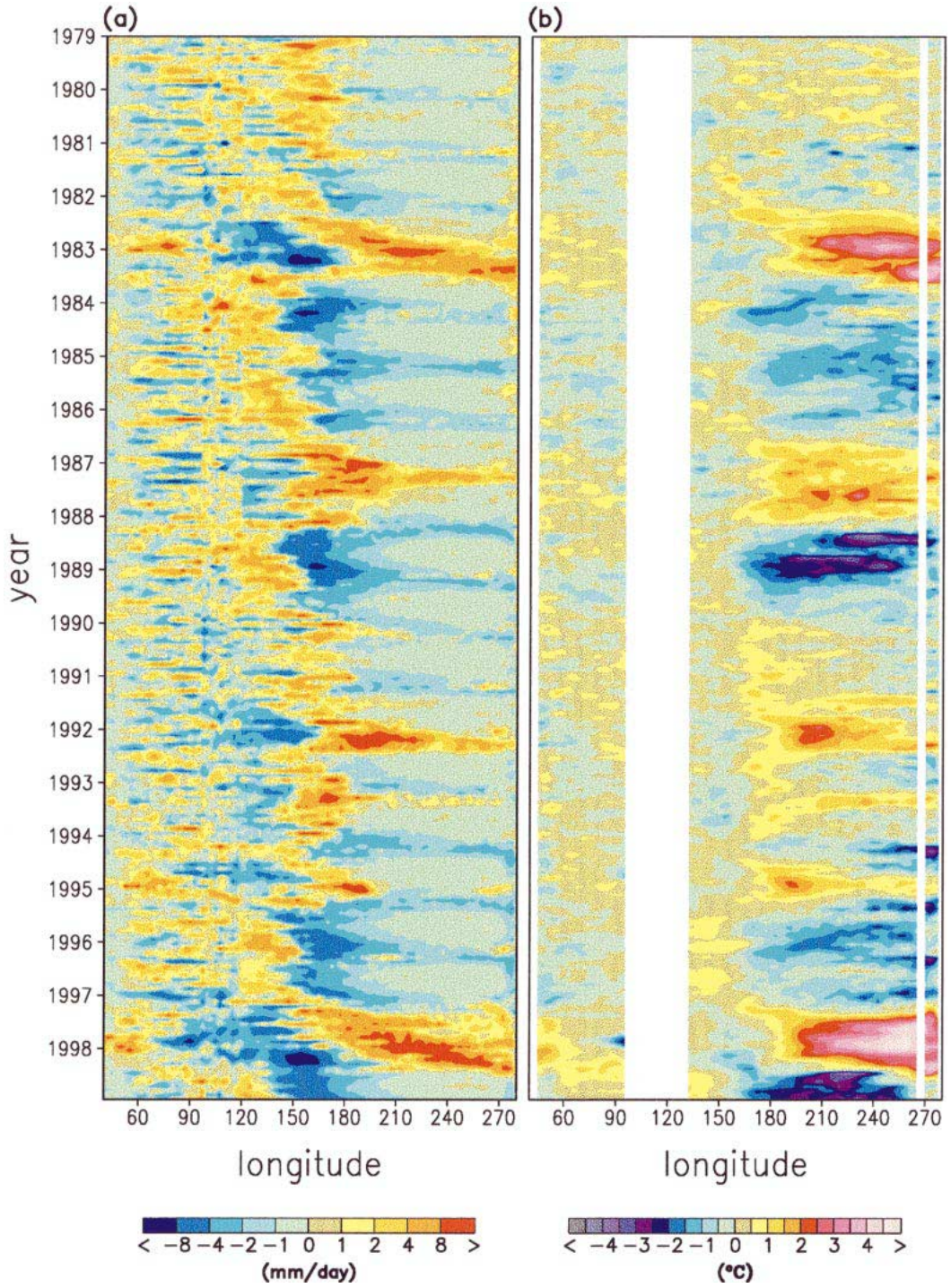

FIG. 2. Time–longitude sections along the equator of (a) monthly rainfall anomalies and (b) monthly SST anomalies for the period 1979–98.

secutive years for some El Niños and not for others? What is the role of the Indian Ocean rainfall–SST dipole in ASM rainfall anomalies? These are complex questions that are not likely to be fully resolved by a single research effort. In this paper, we will explore some answers to these questions.

4. Rainfall–SST coupled modes

To identify the dominant coupled modes of rainfall and SST and to address the specific questions raised in the previous section, we carried out an SVD of the monthly rainfall anomalies over the ASM domain

(20°S–40°N, 30°–150°E) and SST anomaly fields over the global domain (40°S–40°N), from May to September for the period 1979–98. The 5-month period is chosen to capture the monsoon period to the entire ASM domain. To ensure the robustness of the results, the computations have been repeated for various combinations of domains for rainfall and SST. A summary of the impacts of using different spatial and temporal domains will be presented in the appendix. In the course of the analysis, we found an interesting linear trend in the SST and rainfall data. However, since the main focus of this work is on interannual variability, we will defer discussion of the trend to another report. In order to remove any (slight) effect that the trend may have on the results, we first detrend the data before the SVD analysis is applied.

a. SVD1: The basin-scale mode

The first SVD mode (SVD1) is nearly invariant with respect to the choice of domains and represents a truly global mode of rainfall and SST variability that encompasses the entire Tropics (see the appendix). The squared covariance percentage explained by this mode is 47%. In all the subsequent discussions, the signs of the anomalies are taken as shown in the spatial eigenvectors. The actual sign of the anomalies is dependent on that of the corresponding principal component (PC). As shown in Fig. 3a, the rainfall pattern is dominated by negative rainfall anomalies over the western Pacific, Maritime Continent, the equatorial eastern Indian Ocean, and the southern Bay of Bengal, while positive centers are located over the northern Bay of Bengal, southern China, and the western Indian Ocean. The ranges of the rainfall anomalies are of the order of 5–8 mm day^{-1}. This rainfall pattern is a part of the well-known ENSO-related basin-scale east–west dipole with a positive anomaly in the central equatorial Pacific and a negative anomaly over the Maritime Continent (see Fig. 2).

The ASM rainfall pattern is coupled to a basin-scale SST field that is characteristic of the *growth phase* of El Niño in the Pacific (Fig. 3b). When compared with the SST empirical orthogonal functions (EOF), the SVD pattern shows considerably more features over the Indian Ocean and the western Pacific, indicating the influence of ASM. Above-normal and below-normal SSTs are found in the western and eastern Indian Ocean, respectively, creating an east–west SST gradient opposite to that in the Pacific. The warmer water off the coast of East Africa and the Arabian Sea may be an indication of the reduced upwelling associated with a weakened broad-scale monsoon during an El Niño. As shown in Fig. 3c, the PCs of rainfall and SST are highly correlated [coefficient (cc) of 0.78], and correspond well with the occurrences of El Niño and La Niña. Both PCs show strong month-to-month persistence, especially when the coupled signals are strong. Both PCs also show a biennial tendency as evident in sharp reversals of the sign of the anomalies in successive years, especially in 1987–88 and 1997–98, respectively. Notice also that the PCs suggest a very different evolution timescale between the 1982/83 and the 1997/98 events. The former has two successive years (1982 and 1983) of positive deviations followed by two years (1984 and 1985) of negative deviations, whereas the latter shows alternating negative and positive swings in 1996, 1997, and 1998. The implication of these different evolution features on the monsoon–ENSO relationship will be examined in section 6.

Figure 3d shows the regression of the 850-hPa wind vectors (plotted as streamlines, with regions having correlation coefficients exceeding 95% confidence level shaded) against the rainfall PC for SVD1. The main feature is a broad region of divergent flow emanating from the Maritime Continent, with westerlies spanning the entire tropical Pacific, and easterlies over the Indian Ocean. The latter appears to fan out into a double anticyclone over the Bay of Bengal and the southern Indian Ocean. These wind anomalies can be identified with those stemming from an eastward shift of the Walker circulation during an El Niño. The divergent flow and double anticyclone imply reduced atmospheric latent heating accompanied by descending motion over the eastern equatorial Indian Ocean and Maritime Continent, which is dynamically consistent with the large-scale negative rainfall anomalies over there. The anomalous easterly flow over the northern Indian Ocean and the northerly wind flow over the western Indian Ocean are indicative of a weakening of the large-scale south Asian monsoon.

The signature of the anomalous Walker circulation is also clear in the regressed 200-hPa wind field (Fig. 3e), which shows strong upper-level anticyclones straddling easterlies over the equatorial western-central Pacific, and confluence over the Maritime Continent, implying large-scale subsidence there. As evident in the lower- and upper-level flow and in the PCs, the large-scale ASM is strongly reduced in 1982, 1987, and 1997 and enhanced in 1984, 1988, and 1998. The upper-level meridional flow also suggests that enhanced precipitation (rising motion) in the monsoon land regions may be connected to the reduced precipitation (descending motion) in the equatorial Indian Ocean through adjustments of an anomalous local Hadley circulation. The basin-scale nature of this mode is evident in the large span of coherent wind pattern across the entire Indo–Pacific region. The shift in the Walker circulation and the induced changes in ASM rainfall anomalies as reflected in SVD1, may be considered as a *direct* impact of El Niño–La Niña.

b. SVD2: The mixed mode

The second SVD mode (SVD2) accounts for 16% of the squared covariance and is statistically well separated from the higher modes (see row labeled GR in Table

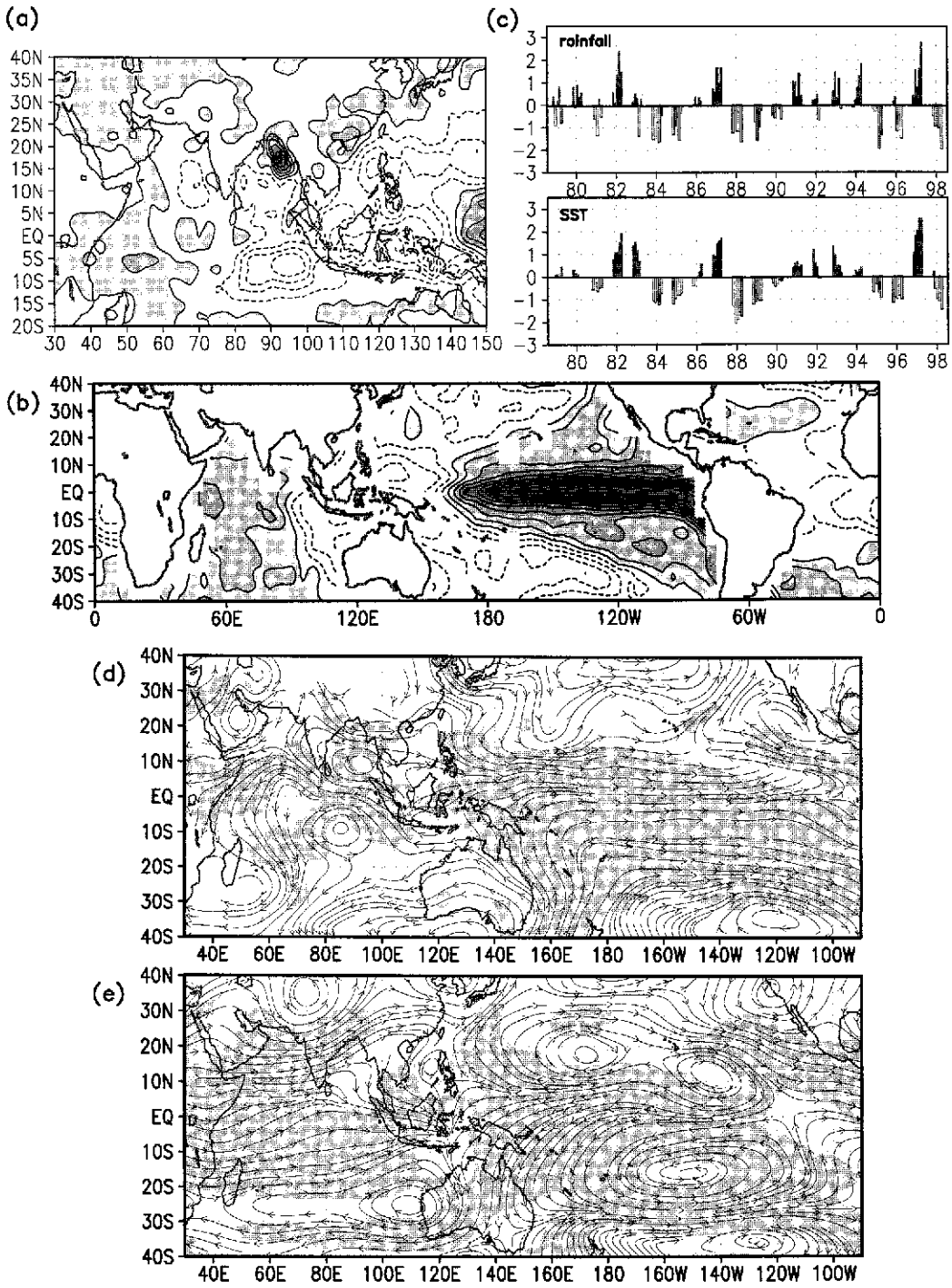

FIG. 3. Spatial and temporal structures of SVD1, based on global SST and ASM rainfall. (a) Singular eigenvector of ASM rainfall for SVD1. Contour interval is 0.5 mm day^{-1}. Regions with positive values are shaded. The range for rainfall anomalies is -6 to 8 mm day^{-1}. (b) Singular eigenvector of SST for SVD1. Contour interval is 0.1°C. Regions with positive values are shaded. The range for SST is $-1°$ to 3°C. (c) Principal components for SVD1 of rainfall and SST in nondimensional units. (d) Streamline based on regression of 850-hPa vector winds against SVD1 rainfall PC with regions exceeding 95% significance shaded, and (e) same as in (d) but for streamline based on regression of 200-hPa vector winds.

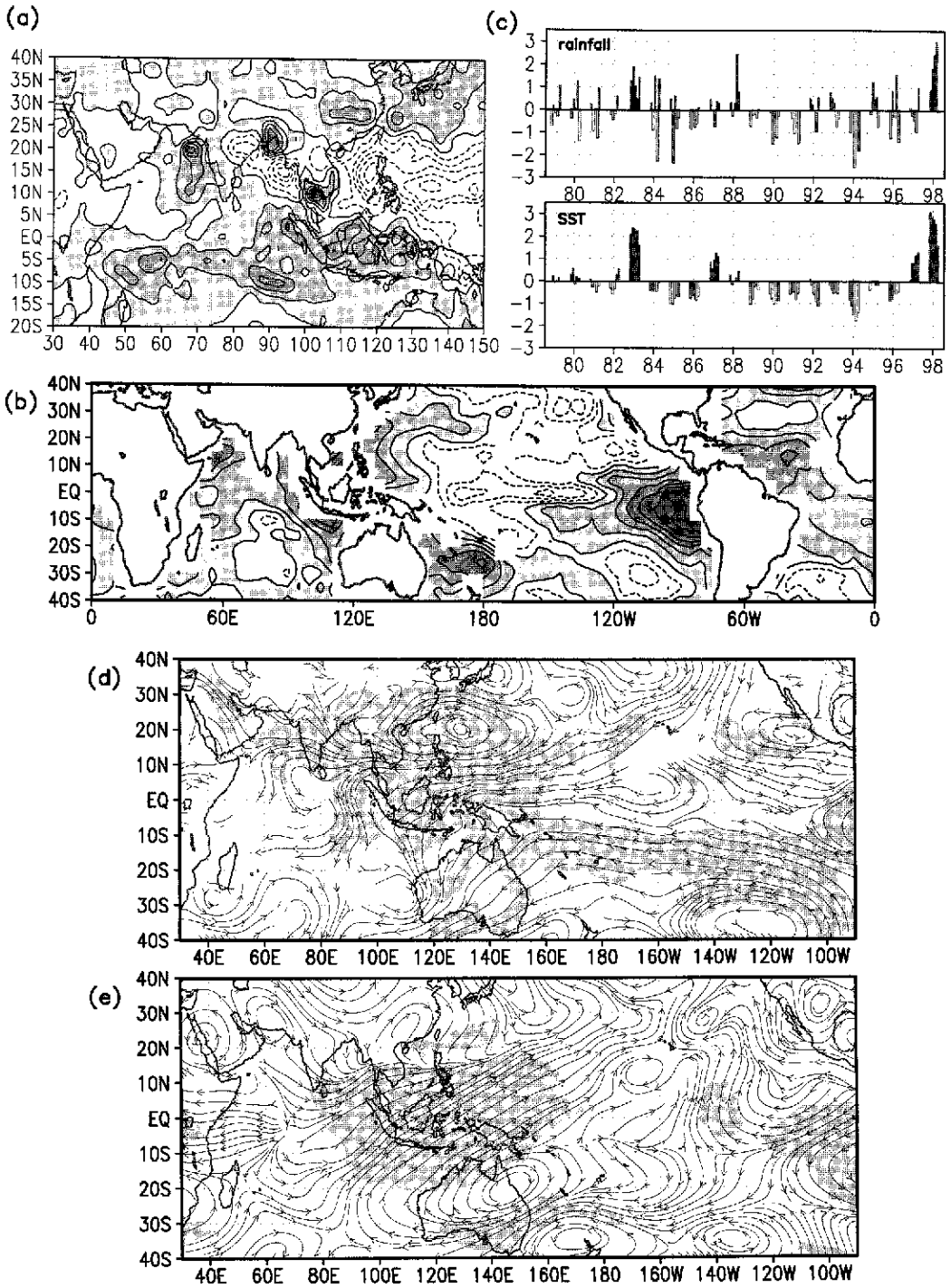

FIG. 4. Same as in Fig. 3, but for SVD2. The range for rainfall is −7 to 7 mm day^{-1} and for SST is −1° to 2°C.

A1). As shown in Fig. 4a, the rainfall pattern features zonally oriented dry and wet belts, with embedded subregional features. The subregional features include positive rainfall anomalies over the Yangtze River Valley and southern Japan (~30°N), the Bay of Bengal, and the eastern Arabian Sea; large negative anomalies over the western Pacific and South China Seas; and positive anomalies in an ITCZ-like structure stretching from the Maritime Continent across the Indian Ocean between the equator and 15°S. This rainfall pattern is coupled to an emerging cold tongue in the equatorial central Pacific, a shrinking warm water region in the eastern Pa-

cific, and an expanding warm pool in the vicinity of the Maritime Continent and the eastern Indian Ocean (Fig. 4b). In contrast to SVD1, the corresponding PCs show only a weak biennial tendency, with episodic variations. The large positive swings in the SST PC in 1983, 1987, and 1998 coincide with the subsequent development of a La Niña (see Fig. 2). The negative swings in the SST PC are generally smaller, but more frequent compared to the positive swings, reflecting an inherent asymmetry in the growth of La Niña.

In contrast to SVD1, the rainfall PC for SVD2 shows quite pronounced month-to-month variability, especially when the SST signal is weak (Fig. 4c). The complex subregional-scale features and the pronounced month-to-month variability in the rainfall pattern suggest that SVD2 is strongly impacted by subseasonal-scale variability, possibly associated with the intraseasonal oscillations, as discussed for Fig. 2. Consistent with the exceptionally large positive deviations of SVD2 in 1998 (Fig. 4c), the rainfall and SST patterns bear strong resemblance to the actual observed ASM rainfall anomaly pattern shown in July 1998 (Fig. 1b). As shown in the appendix, an almost identical SVD2 pattern can be found in an SVD analysis with the 1998 data withheld. This suggests that the 1998 ASM rainfall anomalies may stem from the amplification of a recurring climate mode.

The regressed 850-hPa wind pattern (Fig. 4d) shows a prominent low-level anticyclone over the subtropical western Pacific, northeast of the Philippines, consistent with the reduced rainfall over the region (see Fig. 4a). During the positive phase of this mode (a developing La Niña), the west Pacific anticyclone (WPA) induces strong easterlies from the equatorial western Pacific, across the Bay of Bengal to southern India, and a southwesterly flow into east Asia. The large positive deviations of SVD2 in 1998 suggests that the WPA may be an important mechanism for excessive rainfall over the Yangtze River Valley and over Bangladesh through increased moisture transport from the South China Sea and the western Pacific into these regions. Additionally, the WPA appears to be connected to basin-scale anomalous easterly wind emanating from the southeastern Pacific. The regressed 200-hPa wind (Fig. 4e) shows that the WPA is associated with southwesterly from the Indian Ocean to the western Pacific. A convergence zone between tropical and midlatitude circulation is found around 10°N from the Bay of Bengal to east of the Philippines. This implies sinking motion, consistent with the deficient rainfall over these regions (see Fig. 4a).

The large-scale circulation patterns are similar to those observed for the intraseasonal oscillations in the ASM region (Chen et al. 2000; and Rui and Wang 1990). The coupling of the rainfall and SST PCs are only moderate [correlation coefficient (cc) = 0.59] for this mode. The lower correlation is probably due to the strong subseasonal-scale regional variability inherent in this mode. Because of the presence of both pronounced regional and basinwide features, this mode may be derived from regional coupled SST processes. However the regional processes may not be completely independent of ENSO, because they may be modified by basin-scale SST. In this regard, impacts of El Niño are likely to be *indirect*; that is, through enhancement of local monsoon processes and/or modification of the El Niño forcings. Henceforth we shall refer to SVD2 as the mixed mode.

c. SVD3: The regional mode

The third SVD mode (SVD3) explains 5% of the squared covariance and is only marginally separated from the higher SVDs. The rainfall pattern (Fig. 5a) shows a series of organized positive and negative centers along 0–5°S, including an east–west dipole over the Indian Ocean. Enhanced rainfall is found in localized regions in a zonal belt between 5° and 25°N stretching from northern India, Indochina, the South China Sea, and the East China Sea. The SST pattern suggests a warmer southeastern Indian Ocean coupled to colder South and East China Sea (Fig. 5b). The presence of wavelike SST structures in the extratropics and the wedge-shaped warm SST in the eastern Pacific suggest some similarity with the decadal mode of SST variability over the Pacific (Knutson and Manabe 1998; Meehl and Arblaster 1998). The decadal tendency of this mode can also be seen in the corresponding PCs (Fig. 5c). During the period from 1979 to 1985, the mode stayed mostly in its positive phase. It switched sign and remained in its negative phase during the mid-1980s to the mid-1990s. The correlation between the rainfall and SST PCs is quite high (cc = 0.68) suggesting the role of ocean–atmosphere coupling.

The regressed 850-hPa wind field for SVD3 (Fig. 5d) shows that there is no significant basin-scale wind correlation over the vast stretch of the central and eastern Pacific. Significant wind correlation is confined to the ASM region only. The low-level WPA (shown in its negative phase as a cyclone in Fig. 5d) is again a prominent feature, with its center shifted slightly northeastward in comparison with that in SVD2. The westerly flow in the southern flank of the WPA appears to connect regions of enhanced precipitation shown in Fig. 5a. The easterly flow in the northern flank, just south of Japan, appears to be related to the cold SST found over there. Overall the orientation and extent of the WPA suggests a linkage with the underlying SST pattern in the subtropical central Pacific. At the upper level (Fig. 5e), a northeasterly flow with strong cross-hemispheric meridional flow is found between 100° and 140°E. The directions of the low-level and upper-level flow over the eastern Indian Ocean and the western Pacific indicate that there is a possible interhemispheric connection with the wintertime circulation of the Southern Hemisphere.

As explained in the next section, although the SVD3

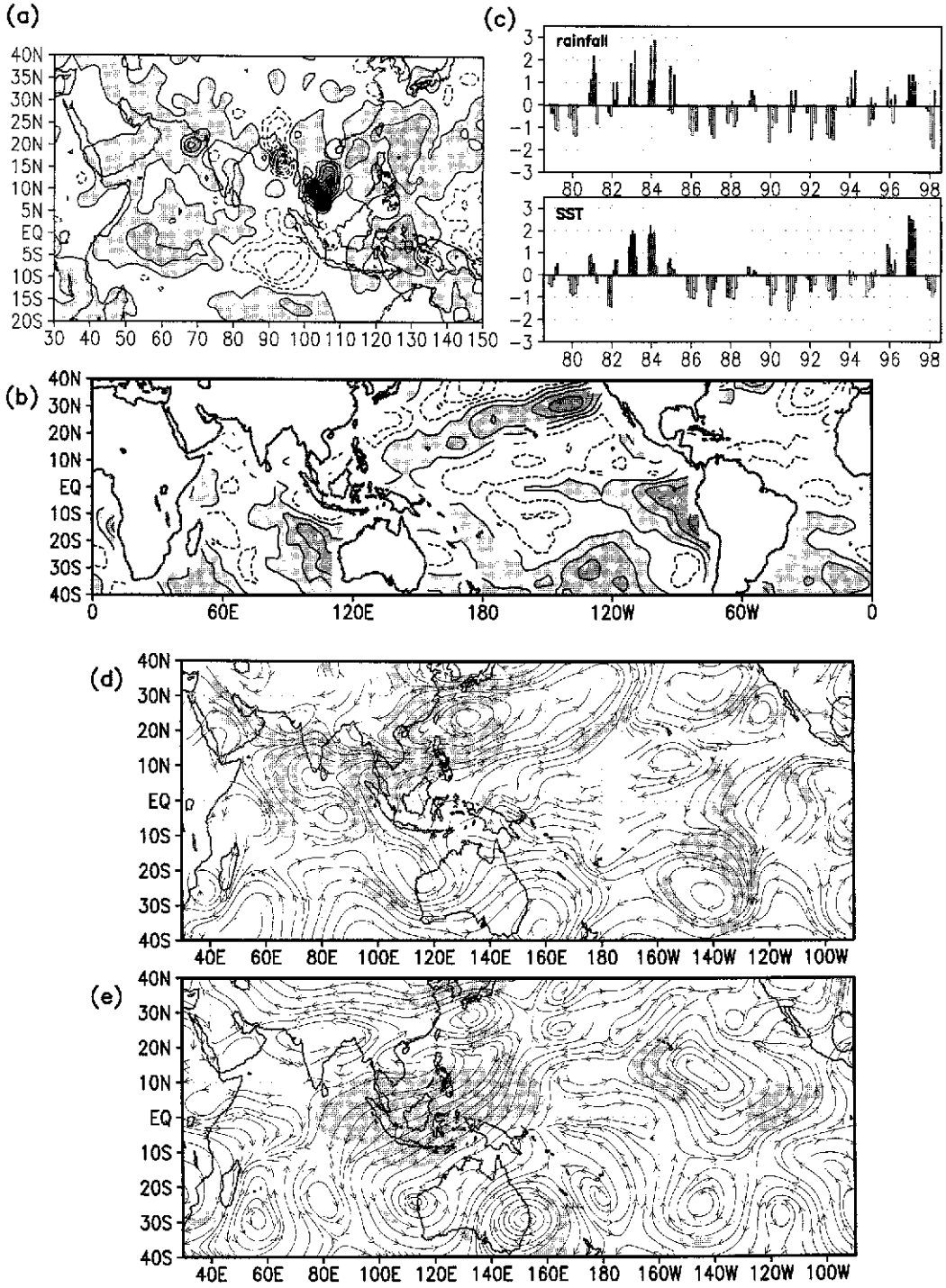

FIG. 5. Same as in Fig. 3, but for SVD3. The range for rainfall is −12 to 15 mm day^{-1} and for SST is −1° to 1°C.

and higher modes (not shown) may explain a relatively small amount of covariance over the entire period, for individual years, SVD3 and higher-order modes may contribute significantly to the ASM rainfall anomaly. Webster et al. (1999) and Saji et al. (1999) find a similar dipole in rainfall and SST in the Indian Ocean during September–November. This may be one of the reasons for the weak signal of this regional mode found here. The spatial and temporal structures of SVD3 are quite robust with respect to the choice of the rainfall and SST domains, with or without the 1998 event (see the appendix).

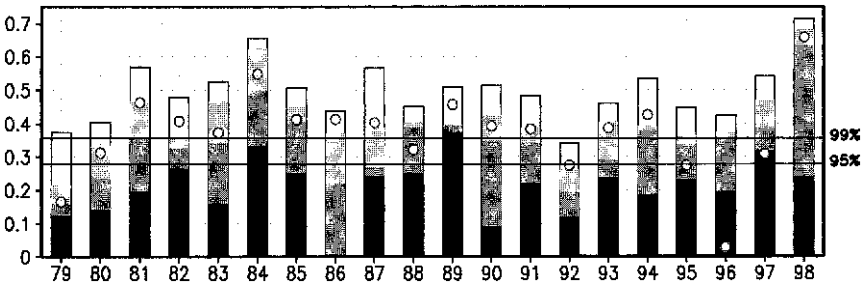

FIG. 6. Year-by-year CAC between reconstructed (based on rainfall PCs) and observed ASM rainfall. Black bar denotes contribution by SVD1. Incremental contributions by SVD2, SVD3, SVD4–5, are indicated by gray, light gray, and white bars, respectively. Open circles denote the CAC level for the first five SVD modes based on the SST PCs.

5. Reconstruction of ASM rainfall anomalies

This section is devoted to the evaluation of the contribution of various physical processes to the observed ASM rainfall anomalies on a yearly basis. Using the procedure as described in Lau and Wu (1999), we computed the cumulative anomalous correlation (CAC), defined by

$$\mathrm{CAC}_{i,j} = \left\langle O_j, \sum_{k=1}^{i} \mathrm{SVD}(k) \times \mathrm{PC}(k)_j \right\rangle, \qquad (1)$$

where, j is the year index; $\langle\ \rangle$ denotes the normalized pattern correlation over a chosen domain between the observed rainfall O_j and the reconstructed rainfall pattern using up to the ith rainfall SVD vector. The incremental contribution to the anomaly correlation by each mode is given by $A_{1,j} = CAC_{1,j}$, $A_{2,j} = CAC_{2,j} - CAC_{1,j}$, and so on. Since the CAC is a measure of the similarity of the reconstructed rainfall field to the observed, we consider it an upper bound on the predictability of the ASM rainfall.

Based on the explained covariance, it is likely that a major portion of the predictability may reside in the first two SVD modes and to a lesser degree also in SVD3. Inspection of the mode-by-mode contribution to the reconstructed rainfall field (not shown) indicates that SVD4 and SVD5 may contribute to realistic subregional features that significantly increase the CAC in some years. However, the higher-order (>5) modes are increasingly variable, containing small-scale features that are unlikely to have any predictability. This is also evident in the fact that the contribution to the CAC in most cases levels off after the 4th and the 5th SVD modes. Therefore, we will consider the CACs only up to the 5th SVD mode as the potential predictability in the following discussions. Note that in (1), either the rainfall PCs or the SST PCs can be used. If the rainfall PC is used, the potential predictability refers to that which is inherent in the ASM rainfall itself, including the contribution from non-SST effects. When the SST PCs are used in (1), the CAC provides a measure of the ASM rainfall potential predictability due to SST only. The potential predictability computed from the SST PCs is almost always less than that from the rainfall PCs because of the imperfect correlation of the SST and the rainfall fields. We consider these two estimates to be the lower and upper bound of the potential predictability.

a. All-ASM domain

Figure 6 shows the CAC for up to the 5th SVD mode each year for the entire ASM domain. The incremental contribution of each mode to the observed rainfall variability is shown by the length of the vertical bars, with a different shade for each mode. We have also estimated the effective number of degrees of freedom of the rainfall field in the ASM domain to be $N^* - 1$, where N^* is the number of EOF modes required to explain 90% of the total variance for all the grid points (Bretherton et al. 1999). This gives 50 effective degrees of freedom for the ASM domain. The correlation coefficients for the 95% and 99% confidence level (cl) based on a two-tailed Student's t test are 0.28 and 0.36, respectively. On the average, the direct impact of the basin-scale SST anomalies (SVD1) ranges from 0.1 to 0.3, mostly falling below the 95% cl, except in 1984, 1989, and 1997. When the mixed mode (SVD2) is included, the CAC increases to the 0.3–0.4 range and generally rises above the 95% cl. It reaches or rises above the 99% cl in 9 out of the 20 yr. For all years, the contribution of the regional modes (SVD3 to 5) to the CAC is in the range 0.1–0.2, certainly nonnegligible in comparison with SVD1 and SVD2. In order to reach potential predictability at CAC values of 0.45 or higher (>99.9% cl), the contributions of the regional modes must be included, except in years of strong La Niña, that is, 1984 and 1998, when the first two modes suffice. The basin-scale contributions from SVD1 and partly from SVD2 are generally larger in the developing phase of La Niña; that is, 1984, 1988, and 1998 in comparison with the developing El Niño, that is, 1982, 1987, and 1997.

The potential predictability (CAC up to the 5th mode) calculated with the rainfall PC for all years, as shown in Fig. 6, has a mean value of 0.45. This value is reduced to 0.37 when we use the SST PC (instead of the rainfall

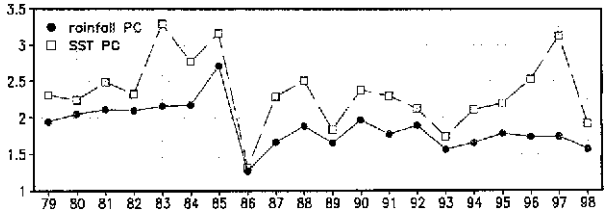

FIG. 7. Year-by-year error variance of the reconstructed ASM rainfall based on the first five rainfall singular vectors, and principal components of rainfall and SST, respectively.

PC) in the CAC computation. As stated before, these numbers can be considered as the upper and lower bounds of potential predictability of the ASM monsoon. A mode-by-mode decomposition shows that much of the SST-based potential predictability is contributed by the first three modes. This is also evident in Fig. 6, in which the SST-based potential predictability generally rise only to the level of the rainfall-based CAC for the first three SVD modes.

Figure 7 shows the year-to-year error variance of the reconstructed ASM rainfall (based on the first five SVD modes) derived from the rainfall and the SST PCs, respectively. It is obvious that the error variances based on rainfall PCs are reduced substantially (20%–30%) from those based on the SST PCs. The result implies that there may be additional sources of predictability based on the non-SST-related regional processes, provided of course that the rainfall modes themselves are predictable. Notice that the differential error variance is very large in 1997 and much smaller in 1998. In other words, much of the ASM rainfall anomalies in 1997 is due to regional processes not coupled to SST, while in 1998 coupled SST processes play a dominant role. These results are consistent with recent studies that suggest during 1997 much of the rainfall variability over the Indian subcontinent was due to the influence of pronounced intraseasonal oscillations and the excitation of regional features, rather than as a direct response to the shift of the Walker circulation (Shen and Kimoto 1999; Slingo and Annamalai 2000).

b. ASM subdomains

In this section, we assess the potential predictability (as measured by the CAC) of the two key subdomains of the ASM; that is, the south Asian monsoon (10°–30°N, 70°–100°E) including the Bay of Bengal, and the east Asian monsoon (10°–35°N, 100°–140°E). These two subdomains are shown as outline boxes in Fig. 1. The number of degrees of freedom is estimated as 21 and 25 for the SAM and EAM, respectively.

Figure 8 shows the yearly variation of the mode-by-mode CAC based on rainfall PCs for the two subdomains. Also shown is the CAC for the first five modes using the SST PCs. It is obvious that the potential predictability of SAM is impacted strongly by SVD1 (the Walker circulation) more so than EAM. The CAC for SAM from SVD1 has a wide range (0–0.6) of year-to-year variability. The CAC contribution by SVD1 alone exceeds or is close to the 99% cl (=0.56) only in 3 out of the 20 yr, that is, 1984, 1987, and 1989. All of these years correspond to occurrences of La Niña. Somewhat surprisingly, there is no contribution from the Walker circulation to the potential predictability of SAM for 1982 and 1997; both years represent the growth phase of El Niño. During these two years, the rainfall variability of SAM is mainly due to regional processes not directly linked to ENSO. In the developing cold phase, 1983/84 and in 1998, the Walker circulation and the

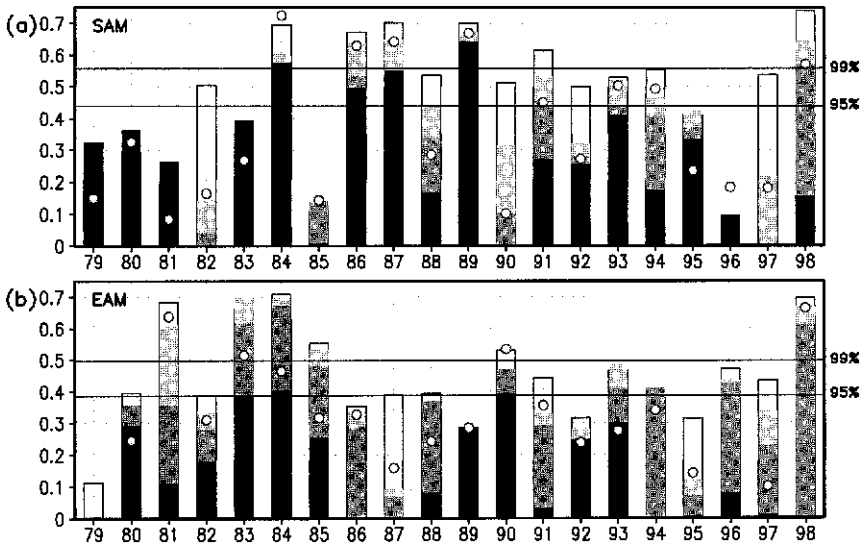

FIG. 8. Same as in Fig. 6 but for the subdomain of (a) SAM and (b) EAM. See text for definition of the subdomains.

WPA (SVD1 and 2 combined) have much larger impacts. In 1998, SVD2 (WPA) has a strong influence on rainfall variability of SAM. The contributions from SVD1 in the 1990s seem to be smaller in comparison with those in the 1980s. The smaller contributions in the 1990s may be related to the weakening in the relationship between the Indian monsoon rainfall and ENSO in the recent decade, which is attributed to a large-scale, secular shift of the Walker circulation (Kumar et al. 1999; Krishnamurthy and Goswami 2000). When the SST PCs are used in the CAC computation, there is a general reduction in the potential predictability. The mean value drops from 0.47 based on rainfall PCs to 0.35 based on SST PCs.

For EAM, the influences of both SVD1 (Walker circulation) and SVD2 (WPA) are quite obvious, with the latter having slightly more influence. Here, the time-mean potential predictability from the first five SVD modes is 0.45, slightly less than that of the SAM. Substantial increase in potential predictability (CAC > 0.5) by the first two modes occurs in 1983, 1984, and 1998. In 1998, the WPA alone accounts for approximately 0.6 of the CAC, suggesting an exceptionally strong influence by the WPA. The CAC exceeds the 95% cl ($=0.39$) for slightly more than half of the years. The declining influence of the Walker circulation (SVD1) on the EAM and the increasing influence of the WPA (SVD2) in the 1990s are also noted. Since SVD2 is a mixed mode with strong regional characteristics, it may be inferred from Fig. 8 that regional processes play a more important role in rainfall anomalies of the EAM than SAM. When the CAC is computed based on SST PC, the time-mean potential predictability drops to 0.29, which is considerably smaller than the SAM counterpart (0.35). The results suggest that in the long run, it may be more difficult to predict EAM rainfall than SAM rainfall, based on SST alone. An alternate but more positive view is that there may be inherent non-SST-related predictability that could be further exploited in the rainfall modes.

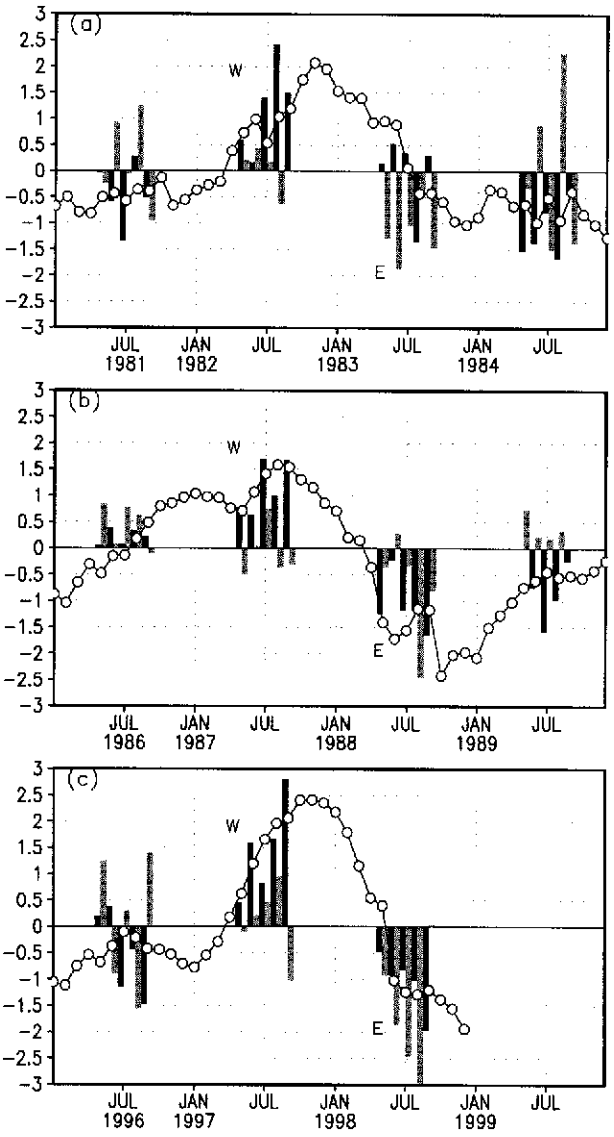

FIG. 9. Time series of Niño-3.4 SST during 1981–84, 1986–89, and 1996–98, showing relationship of SST variation (°C) to PCs for SVD1 (black bar) and SVD2 (gray bar). Positive (negative) values denote westerly (easterly) wind anomalies in the western Pacific.

6. A hypothesis

In previous sections, we have noted that the evolution of the El Niño–La Niña cycles during 1982/84 and 1997/98 are quite different and that their impacts on the ASM and its subdomains are also different. Here, we address the converse problem and explore the hypothesis that the 1982/84 and the 1997/98 El Niño–La Niña evolved differently *because* the wind forcings by the ASM on the El Niños were different. Figure 9 shows the Niño-3.4 SST variation, and the rainfall PCs for SVD1 and SVD2 for years 1981–84, 1986–1989, and 1996–1998, which include the complete life cycle of the three major ENSO in the past 20 years. The sign of the PC for SVD2 has been reversed, so that a positive (negative) sign in both PCs denotes anomalous westerlies (easterlies) in the equatorial western Pacific. As noted in previous discussions and from the Niño-3.4 SST time series, the 1982/83 event (Fig. 9a) had a longer cycle, with the cold and warm phases lasting about four years, whereas the 1997/98 event (Fig. 9c) had a much shorter cycle of approximately two years. During MJJAS 1982, SVD1 was large and positive, indicating prevailing low-level westerly wind over the Pacific induced by the eastward shift of the Walker circulation. This westerly wind increase would most likely lead to excitation of eastward-propagating oceanic Kelvin waves, contributing to the development of El Niño (Kessler et al. 1995). Since SVD2 was weak, the WPA contributed very little to the warming in 1982. As the Niño-3.4 SST evolved, it peaked around October–December 1982. The turnaround

may be related to the possible enhancement of the WPA in the winter following the growth phase of El Niño (Wang et al. 1999). In the following summer (1983), SVD2 (WPA) contributed strong low-level easterlies over the western Pacific. This easterly wind was, however, opposed by a westerly wind remaining from the warm event; that is, the Walker circulation remained shifted eastward from its climatological position, resulting only in a weak cold event in 1984. During JJA 1984, the strong contribution from SVD1 and partially from SVD2 produced easterly wind over the western Pacific, leading to a prolonged cold phase in 1984/85.

Figure 9c shows that the growth phase of the 1997/98 El Niño was similar to that of 1982/83, in that the eastward shift of the Walker circulation (SVD1) was mostly responsible for the rapid warming. Similar to 1982, the Niño-3.4 SST peaked in October–December, 1997. However, the decay phase of El Niño evolved very differently between the two cases. From May to September 1998, both the Walker circulation and the WPA were strong and extremely coherent. They combined to produce very strong easterly wind anomalies over the western Pacific. As a result, the El Niño rapidly terminated and La Niña emerged within 12 months, implying a distinct biennial signal. The aforementioned interplay between the Walker circulation and the WPA, in relation to Niño-3.4 SST variation appeared to also fit the 1987/88 event (Fig. 9b), which was similar to the 1997/98 event in having a well-defined La Niña, immediately following the El Niño. Hence it is plausible that not only does the El Niño have an impact on the ASM but wind anomalies derived from ASM variability may have a strong impact on the evolution of El Niño–La Niña cycles.

7. Concluding discussion

Using 20 yr of rainfall and SST data, we identified natural modes of variability in the Asian monsoon region and explored their physical underpinnings. Using these natural modes, we assessed the role of monsoon–ENSO coupling and other physical processes in contributing to rainfall variability over the all-Asia monsoon domain, as well as the south Asia and the east Asian subdomains.

We found three natural, recurring coupled modes that may play important roles in interannual variability of the ASM rainfall. The most dominant coupled mode (SVD1) accounts for 47% of the covariance, and is characterized by a basinwide coherent pattern, associated with the east–west shifts of the Walker circulation and SST anomaly patterns across the equatorial Indo–Pacific basin that occur during the transition phases of El Niño and La Niña. In this mode, the ASM rainfall is affected by large-scale sinking (rising) motions over the equatorial eastern Indian Ocean and Maritime Continent associated with the anomalous Walker circulation. SVD1 differs from the traditional ENSO SST mode in that it emphasizes the strong biennial tendency in ASM rainfall and global SST, and captures the symmetric component of the transition between the warm and cold phases and vice versa. This mode constitutes the direct impact of ENSO on the ASM.

The second mode (SVD2) is interpreted as a mixed mode with attributes of both basinwide and regional processes including large month-to-month variability. SVD2 accounts for approximately 16% of the total covariance, and features an anomalous low-level anticyclone in the subtropical western Pacific, off the coast of east Asia. This anticyclone is coupled to a developing anomalous warm pool in the oceanic regions adjacent to the ASM landmasses and an emerging cold tongue in the equatorial central Pacific during the growth phase of a La Niña. During 1998, SVD2 had a very strong influence on rainfall anomalies over east Asia and the south Asia region. This mode may be considered as the ''indirect'' impact of ENSO on ASM in that it is governed by regional monsoon coupled processes that may stem from strong interactions with the direct response.

The third mode (SVD3), which accounts for only 5% of the rainfall–SST covariability, consists of a rainfall dipole in the Indian Ocean just south of the equator, coupled to a northwest–southeast-oriented SST anomaly in the southern Indian Ocean. SVD3 may be associated with decadal-scale fluctuation of the west Pacific anticyclone. This mode exhibits features that are suggestive of coupling with extratropical circulation in the North Pacific and regional interhemispheric teleconnections between the Australian wintertime circulation and ASM.

An analysis based on cumulative anomaly correlation shows that for the all-ASM domain, in addition to basin-scale or ENSO-related impacts, regional processes play an important role in determining ASM rainfall variability and potential predictability. Potential predictability based on SST can account for only 0.35 and 0.29 of the rainfall variability for the south Asian monsoon and east Asian monsoon, respectively. The former is affected more by the east–west shift in Walker circulation, the latter more by the WPA. We found that there is little impact from basin-scale SST forcings (SVD1 and SVD2) on rainfall anomalies for the south Asian monsoon in 1997. Any impacts may have been masked or opposed by strong regional processes in that region. The extraordinary rainfall anomalies in EAM in 1998 may have stemmed from the indirect response to a growing La Niña in the form of excitation of a recurring intrinsic coupled climate mode (SVD2), amplified by regional-scale processes.

Our results suggest that strong monsoon–ENSO connection tends to occur with a pronounced 2-yr polarity switch in basin-scale SST anomalies, that is, the transition phases, so that the monsoon–ENSO relationship needs to be considered in pairs of years, in relationship to the evolution of SST. Based on these results, we propose a possible mechanism in which the ASM may induce a strong biennial signal, modulating the timescales of

ENSO cycles. We argue that in addition to the well-known east–west shift of the Walker circulation associated with El Niño–La Niña transition, the western Pacific anticyclone may be a crucial link that determines how biennial and intraseasonal oscillations may influence monsoon–ENSO interactions. The full interaction of monsoon and the ENSO cycles, however, is likely to involve both the winter and summer components of the Asian–Australian monsoon.

We point out the results of this paper are based on data for the last two decades and, therefore, may not be applicable for other decades. There is now a growing body of evidence that the monsoon–ENSO relationship historically has waxed and waned on interdecadal or longer timescales and is likely to continue to evolve in future decades. Increased knowledge of its fundamental nonstationary nature will be a key to a better understanding of monsoon–ENSO relationship.

Acknowledgments. This work is supported jointly by the NASA Global Modeling and Data Analysis Program, and the TRMM project. Comments from two anonymous reviewers have much improved the organization of this paper.

APPENDIX

Computations Using Different Spatial and Temporal Domains

a. SVD analyses for different spatial domains

In this appendix, we present select results of additional computations using different spatial and temporal domains. As stated in the main text, the global region is defined as the entire Tropics from 40°S to 40°N and ASM regional domain as the latitude–longitude limits of (20°S–40°N, 30°–150°E). The SVD results discussed in the main text are then referred to as global SST–regional rainfall domain (GR). Three additional SVD calculations were carried out using the global SST and global rainfall (GG), regional rainfall and regional SST (RR), and remote SST and regional rainfall (ReR), where the remote region is defined as the entire Tropics minus the ASM domain. This different combination of domains is to ensure that the results for the SVD modes are robust. Table A1 shows the percentage of squared covariance explained by the first five modes in all the different calculations. The relative dominance of SVD1 in comparison with the higher-order modes is obvious in all the computations. The spatial pattern of SVD1 depicting the shift of the Walker circulation is essentially independent of the choice of domains, reconfirming that it is a truly global mode. The SVD2 is well separated from the higher modes in all cases. The main features in the SVD2 mode including the WPA are also captured by all the different SVD calculations. The third mode (SVD3), which is interpreted as the regional mode, has the highest percentage covariance explained in RR (8%) in comparison with the rest. Figure A1 shows the spatial pattern of SVD3 in RR, which should be compared with Fig. 5 for GR. The prominent features are the following: a rainfall dipole in the Indian Ocean, positive SST anomalies in the southeastern Indian Ocean, and colder water surrounding the Maritime Continent and eastern Indian Ocean.

TABLE A1. Percentage of squared covariance explained by the first five SVD modes of monthly rainfall and SST for MJJAS for various domains: GG, GR, ReR, and RR. See appendix text for definitions of the domains.

	SVD1	SVD2	SVD3	SVD4	SVD5
GG	57	14	3	3	3
GR	47	16	5	4	3
ReR	53	15	5	3	3
RR	36	26	8	6	4
GR (excluding 1998)	50	9	5	4	4

b. Impact of the 1998 event

To ensure that the large rainfall and SST anomalies in 1998 do not dominate the results of this paper, we have recomputed the SVD with the GR domain and with 1998 removed. The amount of covariability accounted

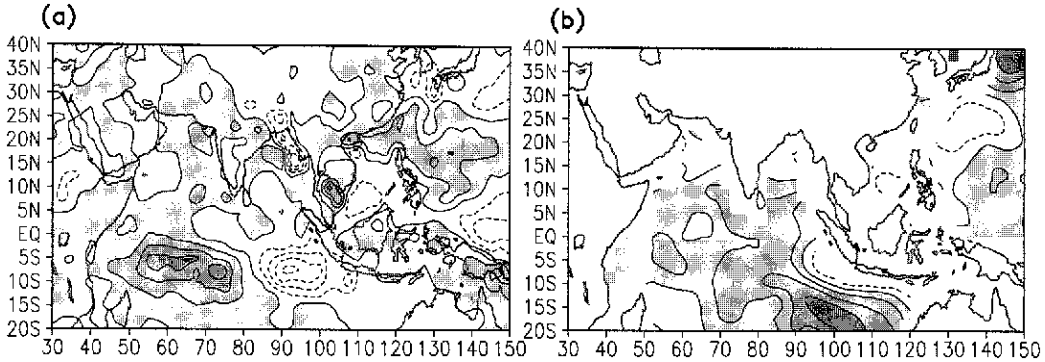

FIG. A1. Spatial pattern of (a) rainfall and (b) SST associated with SVD3, based on RR. Contour interval is 0.5 mm day^{-1} for rainfall and 0.1°C for SST.

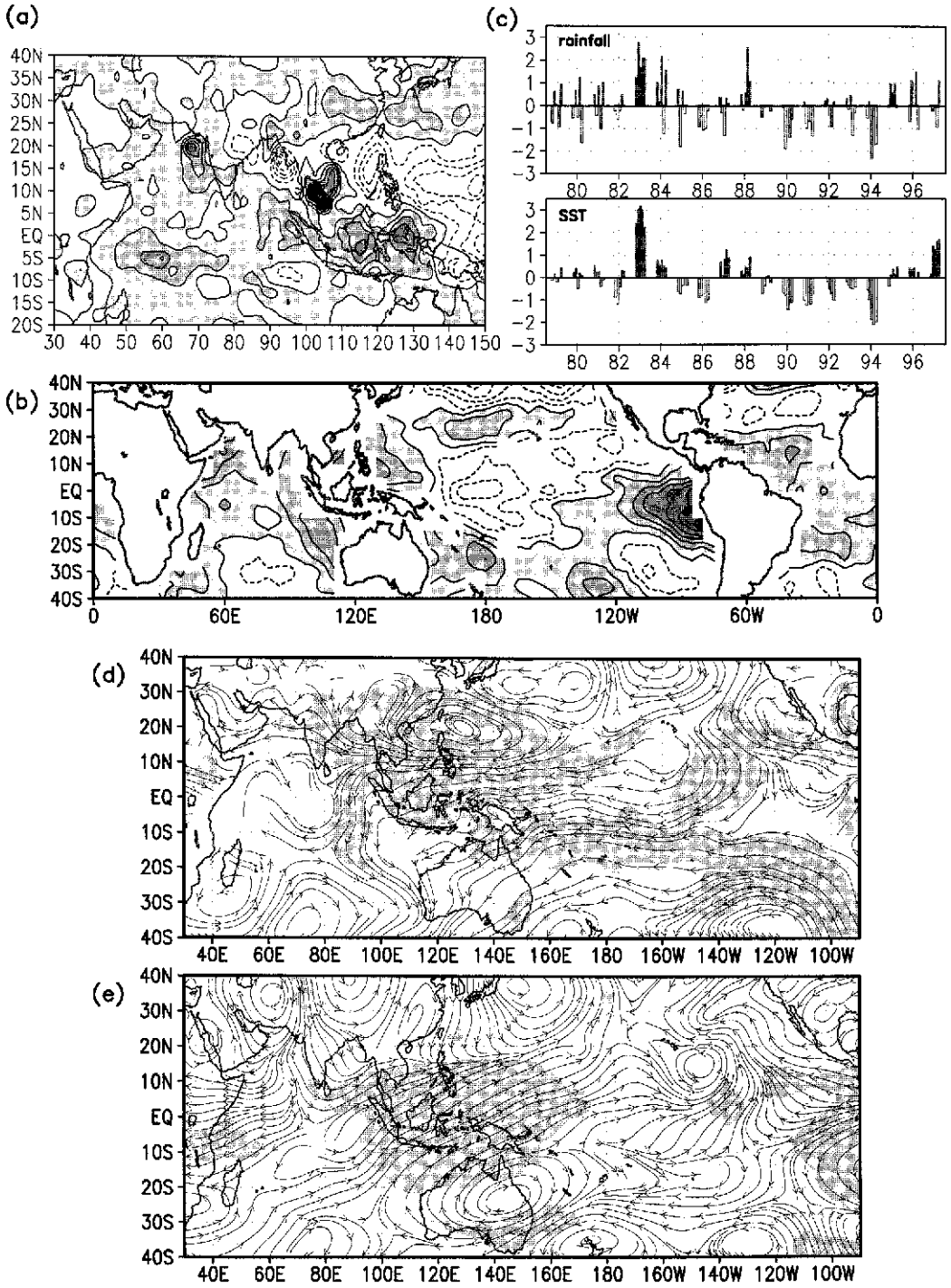

FIG. A2. Spatial and temporal structure of SVD2 based on 19 years (1979–97). (a) Singular eigenvector of ASM rainfall for SVD2. Contour interval is 0.5 mm day^{-1}. (b) Singular eigenvector of SST for SVD2. Contour interval is 0.1°C. (c) Principal components for SVD2 of rainfall and SST in nondimensional units. (d) Streamline based on regression of 850-hPa vector winds against SVD2 rainfall PC with regions exceeding 95% significance shaded, and (e) same as in (d) but for streamline based on regression of 200-hPa vector winds.

for by SVD1 increases to 50% and that for SVD2 reduces to 9% (see bottom row of Table A1). Most important, all the main features contained in the first three leading modes remain essentially unchanged. As an example, Fig. A2 shows the rainfall, SST, and regressed wind for SVD2, which should be compared with Fig. 4. Also noteworthy is the strong similarity of the rainfall pattern in Fig. A2a to the observed rainfall anomaly in July 1998 (Fig. 1b). This result further attests to the interpretation that the major anomalies found in the ASM region in 1998 stemmed from the indirect response to a growing La Niña in the form of excitation of a recurring intrinsic coupled climate mode, amplified by regional-scale processes.

REFERENCES

Bretherton, C. S., M. Widmann, V. P. Dymnikov, J. M. Wallace, and I. Blade, 1999: The effective number of spatial degrees of freedom of a time varying field. *J. Climate,* **12,** 1990–2009.

Chandrasekar, A., and A. Kitoh, 1998: Impact of localized sea surface temperature anomalies over the equatorial Indian Ocean on the Indian summer monsoon. *J. Meteor. Soc. Japan,* **76,** 841–853.

Chen, T. C., M. C. Yen, and S.-P. Weng, 2000: Interaction between the summer monsoons of East Asia and the South China Sea: Intraseasonal monsoon modes. *J. Atmos. Sci.,* **57,** 1373–1392.

Goswami, B. N., D. Sengputa, and G. Sureshkumar, 1998: Intraseasonal oscillations and interannual variability of surface winds over the Indian monsoon region. *Proc. Indian Acad. Sci.,* **107,** 45–64.

——, V. Krishnamurthy, and H. Annamalai, 1999: A broad scale circulation index for the interannual variability of the Indian summer monsoon. *Quart. J. Roy. Meteor. Soc.,* **125,** 611–634.

Ju, J., and J. Slingo, 1995: The Asian summer monsoon and ENSO. *Quart. J. Roy. Meteor. Soc.,* **121,** 1133–1168.

Kalnay, E., and Coauthors, 1996: The NCEP/NCAR 40-Year Reanalysis Project. *Bull. Amer. Meteor. Soc.,* **77,** 437–471.

Kessler, W. S., M. J. McPhaden, and K. M. Weickmann, 1995: Forcing of intraseasonal Kelvin waves in the equatorial Pacific. *J. Geophys. Res.,* **100,** 10 613–10 631.

Knutson, T., and S. Manabe, 1998: Model assessment of decadal variability and trends in the tropical Pacific Ocean. *J. Climate,* **11,** 2273–2296.

Krishnamurthy, V., and B. N. Goswami, 2000: Indian monsoon–ENSO relationship on interdecadal timescale. *J. Climate,* **13,** 579–595.

Kumar, K., B. Rajagopalan, and M. A. Cane, 1999: On the weakening relationship between the Indian Monsoon and ENSO. *Science,* **284,** 2156–2159.

Lau, K.-M., and S. Yang, 1996: The Asian monsoon and the predictability of the tropical ocean–atmosphere system. *Quart. J. Roy. Meteor. Soc.,* **122,** 945–957.

——, and H. T. Wu, 1999: An assessment of the impact of the 1997–98 El Niño on the Asian–Australian monsoon. *Geophys. Res. Lett.,* **26,** 1747–1750.

——, and H. Weng, 2001: Coherent modes of global SST and summer rainfall over China: An assessment of the regional impacts of the 1997–98 El Niño. *J. Climate,* **14,** 1294–1308.

——, K. M. Kim, and S. Yang, 2000: Internal dynamics and boundary forcing characteristics associated with interannual variability of the Asian summer monsoon. *J. Climate,* **13,** 2461–2482.

Li, C., and M. Yanai, 1996: The onset and interannual variability of the Asian summer monsoon and relation to land–sea thermal contrast. *J. Climate,* **9,** 358–375.

Meehl, G. A., 1997: The South Asian monsoon and the tropospheric biennial oscillation. *J. Climate,* **10,** 1921–1943.

——, and J. Arblaster, 1998: The Asian–Australian monsoon and El Niño–Southern Oscillation in the NCAR climate system model. *J. Climate,* **11,** 1356–1385.

Miyakoda, K., A. Navarra, and M. N. Ward, 1999: Tropical-wide teleconnection and oscillation. II: The ENSO–monsoon system. *Quart. J. Roy. Meteor. Soc.,* **125,** 2937–2963.

Rasmusson, E. M., and T. H. Carpenter, 1983: The relationship between eastern equatorial Pacific sea surface temperature and rainfall over India and Sri Lanka. *Mon. Wea. Rev.,* **111,** 517–528.

Reynolds R. and T. M. Smith, 1994: Improved global sea surface temperature analysis using optimum interpolation. *J. Climate,* **7,** 929–948.

Rui, H., and B. Wang, 1990: Development characteristics and dynamic structure of tropical intraseasonal convection anomalies. *J. Atmos. Sci.,* **47,** 357–379.

Saji, N. H., B. N. Goswami, P. N. Vinayachandran, and T. Yamagata, 1999: A dipole mode in the tropical Indian Ocean. *Nature,* **401,** 360–362.

Shen, S.-H., and K. M. Lau, 1995: Biennial oscillation associated with the East Asian summer monsoon and tropical sea surface temperature. *J. Meteor. Soc. Japan,* **73,** 105–124.

Shen, X., and M. Kimoto, 1999: Influence of El Niño on the 1997 Indian summer monsoon. *J. Meteor. Soc. Japan,* **77,** 1023–1037.

Shukla, J., and D. Paolino, 1983: The Southern Oscillation and the long-range forecasting of monsoon rainfall over India. *Mon. Wea. Rev.,* **111,** 1830–1837.

Slingo, J. M., and H. Annamalai, 2000: The El Niño of the century and the response of the Indian summer monsoon. *Mon. Wea. Rev.,* **128,** 1778–1797.

Torrence, C., and P. Webster, 1999: Interdecadal changes in the ENSO–monsoon system. *J. Climate,* **12,** 2679–2710.

Wang, B., and Z. Fan, 1999: Choice of South Asian summer monsoon indices. *Bull. Amer. Meteor. Soc.,* **80,** 629–638.

——, R. Wu, and X. Fu, 2000: Pacific–East Asian teleconnection: How does ENSO affect East Asian climate? *J. Climate,* **13,** 1517–1536.

Webster, P. J., and S. Yang, 1992: Monsoon and ENSO: Selectively interactive systems. *Quart. J. Roy. Meteor. Soc.,* **118,** 877–926.

——, A. Moore, J. Loschnigg, and R. Leban, 1999: Coupled ocean–atmosphere dynamics in the Indian Ocean during 1997–98. *Nature,* **401,** 356–360.

Xie, P., and P. A. Arkin, 1997: Global precipitation: A 17-year monthly analysis based on gauge observations, satellite estimates, and numerical model outputs. *Bull. Amer. Meteor. Soc.,* **78,** 2539–2558.

Yu, L., and M. M. Rienecker, 1999: Mechanisms for the Indian Ocean warming during the 1997–98 El Niño. *Geophys. Res. Lett.,* **26,** 735–738.